IEEE Access
Multidisciplinary ⋮ Rapid Review ⋮ Open Access Journal

Received November 18, 2017, accepted December 18, 2017, date of publication December 28, 2017, date of current version February 28, 2018.

Digital Object Identifier 10.1109/ACCESS.2017.2787839

Composite Controller for Antagonistic Tendon Driven Joints With Elastic Tendons and Its Experimental Verification

MUHAMMAD SHOAIB[1], JOONO CHEONG[1], (Member, IEEE), DONGIL PARK[2], AND CHANHUN PARK[2]

[1]Department of Control and Instrumentation Engineering, Korea University, Sejong 30019, South Korea
[2]Robotics Division, Korea Institute of Machinery and Materials, Daejeon 34103, South Korea

Corresponding authors: Joono Cheong (jncheong@korea.ac.kr) and Chanhun Park (chpark@kimm.re.kr)

This work was supported in part by the Basic Science Research Program through the National Research Foundation of Korea funded by the Ministry of Education, Science and Technology, under Grant 2015R1D1A1A01060319, and in part by the National Research Council of Science and Technology (NST), Korea Government.

ABSTRACT In this paper, we present the dynamic modeling and controller design of a tendon-driven system that is antagonistically driven by elastic tendons. In the dynamic modeling, the tendons are approximated as linear axial springs, neglecting their masses. An overall equation for motion is established by following the Euler–Lagrange formalism of dynamics, combined with rigid-body rotation and vibration. The controller is designed using the singular perturbation approach, which leads to a composite controller (i.e., consisting of a fast sub-controller and a slow sub-controller). An appropriate internal force is superposed to the control action to ensure the tendons to be in tension for all configurations. Experimental results are provided to demonstrate the validity and effectiveness of the proposed controller for the antagonistic tendon-driven system.

INDEX TERMS Tendon-driven system, antagonistic actuation, composite controller, singular perturbation approach.

I. INTRODUCTION

Tendon-driven systems in robotics and machines have several promising features, including light-weight design, a high payload to weight ratio, and re-configurability. However, they also have some significant drawbacks, such as low stiffness, elongation of the tendons, pull-only actuation, and the nonlinear characteristics of tendons that complicate controller design [1]–[3]. The elasticity of tendons in particular plays as a major source of obstacle that prevents from proper mechanical operation [4], [5]. So, in this paper, we propose a reliable controller for tendon-driven systems that guarantees effective tracking performance by reducing the deleterious effects of elastic tendons (*i.e.*, vibrations and jerky movements at the changes in direction), through the use of the singular perturbation approach.

A large number of studies have been conducted with the purpose of optimizing tendon transmission for developing robotic systems such as the whole arm manipulator [6], the astronaut rehabilitative training robot [7], and the ECCE humanoid robot [8], just to name a few. However, the best example of a tendon-driven system may be found in the human body. Most of human's biological joints are driven by the contraction of antagonist and agonist tendons. Unlike the rotary types of tendon-driven joints that are often found in mechanical systems, human joints are driven by tendons that are directly anchored to the sides of bones, which are known as on-link typed joints [9]. The advantages of on-link typed joints over simple rotary joints include increased structural stiffness, better controllability, and enhanced mechanical load-carrying ability, although the increased difficulty of control is a downside that has not yet been completely overcome. In this paper, we focus on the on-link type of tendon-driven joint system, although the theoretical claims can be generalized to other joint types with ease.

Designing adequate controllers dedicated to tendon-driven systems must be an important issue; the use of tendons instead of rigid transmissions leads to new challenges in this respect. For example, because tendons can only pull and not push, the controller must guarantee that all tendons should remain under tension at all times [10]. Another important problem is the elasticity of the tendons, which may cause unwanted vibrations or fluctuations at the discontinuity of accelera-

tion. This is particularly problematic for robotic applications where high precision and accurate tracking performance are required, such as assembly, spraying, aligning, or other manipulations by the end-effector [11]. In order to cope with these issues, a reliable and dependable controller is needed.

Many conventional control techniques, if tendons are treated as non-elastic elements, could be used for tendon-driven systems, including inverse dynamic control [12], [13], robust iterative learning control [14], robust PID and PD control [15], [16], sliding mode control [17], and optimal control [18]. In practice, however, any controller designed under this assumption for rigidity can create instability or failure during high speed motion.

Previous studies on controller design for tendon-driven systems that incorporate the elasticity of the tendons seem very limited (see, for example, [4], [5], [19]). In [4], an inner and outer loop control scheme was proposed, in which an inverse dynamics controller was designed to control the end-effector's pose in the outer feedback loop, while a H_∞ was designed for the inner loop. However, the stability of the system was not fully analyzed. Khosravi and Taghirad [5] proposed a new control strategy by taking into account the elasticity of the tendons. They used the Lyapunov stability theory to analyze system stability, and ensured that all of the cables were in tension at the same time.

While it is important to design controllers for tendon-driven systems with elastic tendons that ensure high precision in positioning and vibration suppression as well, there have not been enough previous examples of controllers that we can evaluate, compare, and adopt. Therefore, in this paper, we propose a novel composite controller based on a two-time scale dynamic model following the singular perturbation approach. The singular perturbation approach has been studied widely in the modeling and control of electro-mechanical systems [20], [21], and has proven its efficacy. This approach may be a unique mathematical and systematic method for dealing with flexible systems, which allows us to extract the slow and fast sub-dynamics and to establish a separate control scheme for each sub-system. The final controller is obtained simply through the linear addition of these two sub-controllers. However, to the authors' best knowledge, its use in tendon-driven systems has been rare, with only a handful of studies, *e.g.*, [22]–[24], having been published on this topic.

This paper, as a new attempt, has three distinct objectives: i) to develop a precise dynamic model of an on-link type antagonistic tendon-driven system with elastic tendons, ii) to obtain the slow and fast subsystems by redefining the dynamic model into the standard form of the singular perturbation approach, and iii) to design and implement a composite controller based on this model. The effectiveness of the proposed control strategy will be demonstrated through experimentation, something which has rarely been conducted on singular perturbation schemes for tendon-driven systems in previous studies.

This paper is organized as follows. First, the kinematics and dynamic modeling of an antagonistic tendon-driven system are described in Section 2. The control and stability of a tendon-driven system with non-elastic tendons is then investigated in Section 3. In Section 4, the effectiveness of the proposed controller is evaluated through experimentation. Finally, concluding remarks are provided in Section 5.

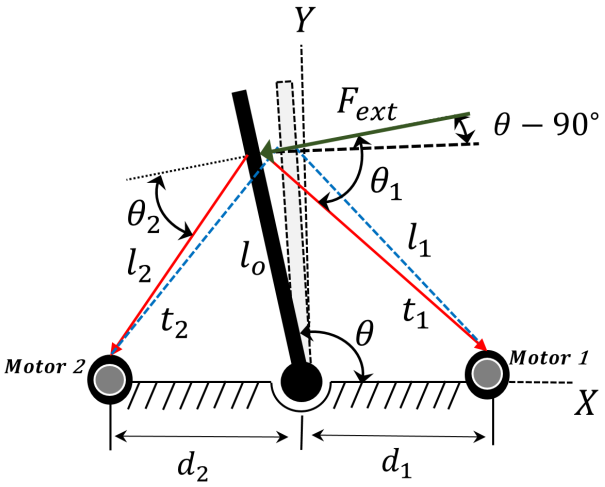

FIGURE 1. Antagonistic tendon-driven joint system with an external force.

II. MODELING ANTAGONISTIC TENDON-DRIVEN JOINT SYSTEMS

A. KINEMATIC MODEL

Fig. 1 displays the schematic of a joint system driven by antagonistic elastic tendons and the exertion of external force F_{ext}, which is normal to the link rotating around the joint. Hereafter, this system will be referred to as the tendon-driven joint (TDJ) system. The dotted and solid lines represent the static equilibrium configurations before and after the exertion of F_{ext}, respectively. We do not consider the force in the axial direction of the link as it would not contribute to the displacement of the joint.

The static equilibrium in Fig. 1 satisfies the equation:

$$-[l_0 \cos\theta_1 \; -l_0 \cos\theta_2] \begin{bmatrix} t_1 \\ t_2 \end{bmatrix} + \tau_{ext} = 0, \tag{1}$$

where l_0 is the length of the link from the base to the point of action for F_{ext}, θ_i, $i = 1, 2$, is the angle between the i-th tendon and the line of action for F_{ext}, t_i, $i = 1, 2$, is the tension in the i-th tendon, and τ_{ext} is the moment at the center of the joint produced by F_{ext}. The above expression can be rewritten as

$$-\boldsymbol{J}^T \boldsymbol{t} + \tau_{ext} = 0,$$

where $\boldsymbol{t} = [t_1 \; t_2]^T$ is the vector for the tensions and $\boldsymbol{J} = [l_0 \cos\theta_1 \; -l_0 \cos\theta_2]^T$ is the structure matrix for this TDJ. We can define the internal force, $\boldsymbol{t}^0 = [t_1^0 \; t_2^0]^T$, such that $t_1^0 \cos\theta_1 - t_2^0 \cos\theta_2 = 0$, which does not contribute to the moment. Based on the virtual work principle, the following also holds:

$$\begin{bmatrix} \dot{l}_1 \\ \dot{l}_2 \end{bmatrix} = \begin{bmatrix} l_0 \cos\theta_1 \\ -l_0 \cos\theta_2 \end{bmatrix} \dot{\theta} \quad \text{or } \dot{l} = \boldsymbol{J}\dot{\theta}. \tag{2}$$

From Fig. 1, it is true that $\cos\theta_i = d_i \sin(\theta - 90)/l_i \quad i = 1, 2$. The above equation can thus be re-written as

$$\begin{bmatrix} \dot{l}_1 \\ \dot{l}_2 \end{bmatrix} = \begin{bmatrix} l_o d_1 \sin\theta/l_1 \\ -l_o d_2 \sin\theta/l_2 \end{bmatrix} \dot{\theta} \quad \text{or } \dot{l} = \boldsymbol{J}\dot{\theta}. \tag{3}$$

The joint stiffness can be expressed as

$$\begin{aligned} K_\theta &:= \frac{d(-\tau_{ext})}{d\theta} = \frac{d\boldsymbol{J}^T}{d\theta}\boldsymbol{t} + \boldsymbol{J}^T\frac{d\boldsymbol{t}}{d\theta} \\ &= \frac{d\boldsymbol{J}^T}{d\theta}\boldsymbol{t} + \boldsymbol{J}^T\boldsymbol{K}^m\boldsymbol{J}, \end{aligned} \tag{4}$$

where Hooke's law for elastic tendons, $\boldsymbol{t} = \boldsymbol{K}^m\delta\boldsymbol{l}$ and $\boldsymbol{K}^m = \text{diag}(K_1^m, K_2^m)$, is applied. By substituting the detailed forms of $\boldsymbol{J}$ and $\boldsymbol{K}^m$ into (4), joint stiffness is expressed as

$$\begin{aligned} K_\theta = l_0^2(K_1^m\cos^2\theta_1 + K_2^m\cos^2\theta_2) \\ - t_1 l_0^2 \sin\theta_1 \frac{d\theta_1}{d\theta} + t_2 l_0^2 \sin\theta_2 \frac{d\theta_2}{d\theta}. \end{aligned} \tag{5}$$

In the above, $d\theta_i/d\theta$ can be obtained from the geometry of Fig.1. That is, the following two relations (by cosine law),

$$\begin{aligned} l_0^2 + l_1^2 - 2l_0 l_1 \sin\theta_1 &= d_1^2, \\ l_0^2 + d_1^2 - 2l_0 d_1 \cos\theta &= l_1^2, \end{aligned} \tag{6}$$

lead to

$$\frac{d\theta_1}{d\theta} = \frac{d\theta_1}{dl_1}.\frac{dl_1}{d\theta} = \frac{l_1 - l_0\sin\theta_1}{l_1}. \tag{7}$$

Similarly, the following result can also be obtained:

$$\frac{d\theta_2}{d\theta} = \frac{d\theta_2}{dl_2}.\frac{dl_2}{d\theta} = -\frac{l_2 - l_0\sin\theta_2}{l_2}. \tag{8}$$

By plugging in (7) and (8), the joint stiffness in (5) becomes

$$\begin{aligned} K_\theta = l_0^2(K_1^m\cos^2\theta_1 + K_2^m\cos^2\theta_2) \\ - t_1 l_0^2 \sin\theta_1 \frac{l_1 - l_0\sin\theta_1}{l_1} - t_2 l_0^2 \sin\theta_2 \frac{l_2 - l_0\sin\theta_2}{l_2}. \end{aligned} \tag{9}$$

The first part of terms on the right hand side is referred to as the material stiffness of the joint, while the other terms are the geometric stiffness of the joint. Note that the human arm takes advantage of this type of TDJ in motion and load carrying.

B. DYNAMIC MODELING OF ANTAGONISTIC TENDON DRIVEN JOINTS

Now we establish a dynamic equation for the TDJ system shown in Fig.1 using Euler-Lagrange formalism. Under the linear axial spring assumption, the potential energy associated with the tendons of the TDJ can be given by

$$\mathcal{U}_{elastic} = \frac{1}{2}K_1^m(l_1(\theta) - l_1(\theta_{m1}))^2 + \frac{1}{2}K_2^m(l_2(\theta) - l_2(\theta_{m2}))^2, \tag{10}$$

where $l_i(\theta)$ denotes the geometric length of tendon i, and $l_i(\theta_{mi})$ is the length of tendon i measured by the angle of motor i (*i.e.*, θ_{mi}), which satisfies

$$l_i(\theta_{mi}) = r\theta_{mi} + l_{i,0}, \tag{11}$$

where r and $l_{i,0}$ are the pulley radius of motor and the length of tendon i at $\theta_{mi} = 0$, respectively. The stiffness coefficients of the tendons in the above equation can be calculated using the conventional formula as follows:

$$K_i^m = E_i A_i / l_i(\theta_{mi}), \quad i = 1, 2, \tag{12}$$

where E_i and A_i denote the Young's modulus and cross-sectional area of tendon i, respectively.

The gravitational potential energy of the TDJ system is

$$\mathcal{U}_{grav} = mgl_{cg}\sin\theta, \tag{13}$$

where m and l_{cg} are the mass and the distance from joint axis to the center of mass of link, respectively and g is the gravitational constant. The kinetic energy of the TDJ system is

$$\mathcal{T} = \frac{1}{2}\left(ml_{cg}^2 + I\right)\dot{\theta}^2 + \frac{1}{2}J_{m1}\dot{\theta}_{m1}^2 + \frac{1}{2}J_{m2}\dot{\theta}_{m2}^2, \tag{14}$$

where I and J_{mi} are the moment of inertia of the link (at the center of mass) and the rotor inertia of motor i, respectively. The Lagrangian $\mathcal{L} := \mathcal{T} - \mathcal{U}_{elastic} - \mathcal{U}_{grav}$ allows us to obtain equations for motion with generalized coordinates $\boldsymbol{q} = [\theta\ \theta_{m1}\ \theta_{m2}]^T$ as shown in (15), at the bottom of this page. where $\tau_{mi},\ i = 1, 2$, is the torque of motor i.

If we define $\delta l_i \triangleq (l_i(\theta) - l_i(\theta_{mi})), i = 1, 2$, the above equation can be re-written in terms of deflection variables. Combining (6) and (11) and then taking the time derivatives, we obtain the relation between the actuator and deflection variables as

$$\begin{aligned} \delta\ddot{l}_1 &= -(l_o d_1 \sin\theta\dot{\theta})^2/l_1^3(\theta) + l_o d_1\cos\theta\dot{\theta}^2/l_1(\theta) \\ &\quad + l_o d_1 \sin\theta\ddot{\theta}/l_1(\theta) - r\ddot{\theta}_{m1}, \\ \delta\ddot{l}_2 &= -(l_o d_2 \sin\theta\dot{\theta})^2/l_2^3(\theta) - l_o d_2\cos\theta\dot{\theta}^2/l_2(\theta) \\ &\quad - l_o d_2 \sin\theta\ddot{\theta}/l_2(\theta) - r\ddot{\theta}_{m2}. \end{aligned} \tag{16}$$

$$\begin{bmatrix} ml_{cg}^2 + I & 0 & 0 \\ 0 & J_{m1} & 0 \\ 0 & 0 & J_{m2} \end{bmatrix} \begin{bmatrix} \ddot{\theta} \\ \ddot{\theta}_{m1} \\ \ddot{\theta}_{m2} \end{bmatrix} + \begin{bmatrix} K_1^m l_o d_1 \sin\theta(l_1(\theta) - l_1(\theta_{m1}))/l_1(\theta) - K_2^m l_o d_2 \sin\theta(l_2(\theta) - l_2(\theta_{m2}))/l_2(\theta) \\ -rK_1^m(l_1(\theta) - l_1(\theta_{m1})) - rK_1^m(l_1(\theta) - l_1(\theta_{m1}))^2/2l_1(\theta_{m1}) \\ -rK_2^m(l_2(\theta) - l_2(\theta_{m2})) - rK_2^m(l_2(\theta) - l_2(\theta_{m2}))^2/2l_2(\theta_{m2}) \end{bmatrix} + \begin{bmatrix} mgl_{cg}\cos\theta \\ 0 \\ 0 \end{bmatrix} = \begin{bmatrix} 0 \\ \tau_{m1} \\ \tau_{m2} \end{bmatrix}, \tag{15}$$

Equivalently,

$$\begin{aligned}\ddot{\theta}_{m1} &= l_o d_1 \sin\theta\ddot{\theta}/rl_1(\theta) - \delta\ddot{l}_1/r - (l_o d_1 \sin\theta\dot{\theta})^2/rl_1{}^3(\theta)\\ &\quad + l_o d_1 \cos\theta\dot{\theta}^2/rl_1(\theta),\\ \ddot{\theta}_{m2} &= -l_o d_2 \sin\theta\ddot{\theta}/rl_2(\theta) - \delta\ddot{l}_2/r - (l_o d_2 \sin\theta\dot{\theta})^2/rl_2{}^3(\theta)\\ &\quad - l_o d_2 \cos\theta\dot{\theta}^2/rl_2(\theta). \end{aligned} \tag{17}$$

By substituting (17) into (15) the equation can be redefined in terms of joint and deflection variables as follows:

$$\begin{aligned}&\begin{bmatrix} ml_{cg}^2 + I & 0 & 0\\ J_{m1} l_o d_1 \sin\theta/rl_1(\theta) & -J_{m1}/r & 0\\ -J_{m2} l_o d_2 \sin\theta/rl_2(\theta) & 0 & -J_{m2}/r \end{bmatrix}\begin{bmatrix}\ddot{\theta}\\ \delta\ddot{l}_1\\ \delta\ddot{l}_2\end{bmatrix}\\ &+\begin{bmatrix} 0\\ J_{m1} l_o d_1 \cos\theta\dot{\theta}^2/rl_1(\theta) - J_{m1}(l_o d_1 \sin\theta\dot{\theta})^2/rl_1{}^3(\theta)\\ -J_{m2}(l_o d_2 \sin\theta\dot{\theta})^2/rl_2{}^3(\theta) - J_{m2} l_o d_2 \cos\theta\dot{\theta}^2/rl_2(\theta)\end{bmatrix}\\ &+\begin{bmatrix} K_1^m l_o d_1 \sin\theta\delta l_1/l_1(\theta) - K_2^m l_o d_2 \sin\theta\delta l_2/l_2(\theta)\\ -rK_1^m\delta l_1 - rK_1^m\delta l_1^2/2l_1(\theta_{m1})\\ -rK_2^m\delta l_2 - rK_2^m\delta l_2^2/2l_2(\theta_{m2})\end{bmatrix}\\ &+\begin{bmatrix} mgl_{cg}\cos\theta\\ 0\\ 0\end{bmatrix} = \begin{bmatrix}0\\ \tau_{m1}\\ \tau_{m2}\end{bmatrix}. \end{aligned} \tag{18}$$

This is the most comprehensive form of the exact dynamic equation for an antagonistic TDJ system. Starting from (18), we now need to convert the original form of the equation into the standard form of the singular perturbation approach, which separates the dynamics into its slow and fast approximate forms. We will then design a composite controller based on the separated subsystems that enhances control performance.

It has often been the case in previous works, for example, [25] and [26], that the singular parameter is defined as the supremum of the inverse of the stiffness matrix:

$$\mu := \sup_i \frac{1}{K_i^m}. \tag{19}$$

By using the singular parameter μ, the variables of interest can be re-scaled such that

$$\delta l_i = \mu\,\delta\tilde{l}_i, \quad K_i^m = \frac{\tilde{K}_i^m}{\mu}, \quad i = 1, 2. \tag{20}$$

Now substituting (19) and (20) into (18) yields

$$\begin{aligned}&\begin{bmatrix} ml_{cg}^2 + I & 0 & 0\\ J_{m1} l_o d_1 \sin\theta/rl_1(\theta) & -J_{m1}/r & 0\\ -J_{m2} l_o d_2 \sin\theta/rl_2(\theta) & 0 & -J_{m2}/r \end{bmatrix}\begin{bmatrix}\ddot{\theta}\\ \mu\delta\ddot{\tilde{l}}_1\\ \mu\delta\ddot{\tilde{l}}_2\end{bmatrix}\\ &+\begin{bmatrix} 0\\ J_{m1} l_o d_1 \cos\theta\dot{\theta}^2/rl_1(\theta) - J_{m1}(l_o d_1 \sin\theta\dot{\theta})^2/rl_1^3(\theta)\\ -J_{m2}(l_o d_2 \sin\theta\dot{\theta})^2/rl_2^3(\theta) - J_{m2} l_o d_2 \cos\theta\dot{\theta}^2/rl_2(\theta)\end{bmatrix}\\ &+\begin{bmatrix} \tilde{K}_1^m l_o d_1 \sin\theta\delta\tilde{l}_1/l_1(\theta) - \tilde{K}_2^m l_o d_2 \sin\theta\delta\tilde{l}_2/l_2(\theta)\\ -r\tilde{K}_1^m\delta\tilde{l}_1 - r\tilde{K}_1^m\mu\delta\tilde{l}_1^2/2l_1(\theta_{m1})\\ -r\tilde{K}_2^m\delta\tilde{l}_2 - r\tilde{K}_2^m\mu\delta\tilde{l}_2^2/2l_2(\theta_{m2})\end{bmatrix}\\ &+\begin{bmatrix} mgl_{cg}\cos\theta\\ 0\\ 0\end{bmatrix} = \begin{bmatrix}0\\ \tau_{m1}\\ \tau_{m2}\end{bmatrix}. \end{aligned} \tag{21}$$

Simply, by setting $\mu = 0$ in (21), a reduced model of the slow subsystem can be obtained, representing the motion with the assumption for rigidity, as follows:

$$\begin{aligned}&(ml_{cg}^2 + I)\ddot{\theta} + mgl_{cg}\cos\theta + \tilde{K}_1^m l_o d_1 \sin\theta\delta\tilde{l}_{1s}/l_1(\theta)\\ &\qquad - \tilde{K}_2^m l_o d_2 \sin\theta\delta\tilde{l}_{2s}/l_2(\theta) = 0, \end{aligned} \tag{22}$$

$$\begin{aligned}&J_{m1} l_o d_1 \sin\theta\ddot{\theta}/rl_1(\theta) + J_{m1} l_o d_1 \cos\theta\dot{\theta}^2/rl_1(\theta)\\ &\qquad - J_{m1}(l_o d_1 \sin\theta\dot{\theta})^2/rl_1^3(\theta) - r\tilde{K}_1^m\delta\tilde{l}_{1s} = \tau_{m1s}, \end{aligned} \tag{23}$$

and

$$\begin{aligned}&J_{m2} l_o d_2 \sin\theta\ddot{\theta}/rl_2(\theta) + J_{m2}(l_o d_2 \sin\theta\dot{\theta})^2/rl_2^3(\theta)\\ &\qquad + J_{m2} l_o d_2 \cos\theta\dot{\theta}^2/rl_2(\theta) + r\tilde{K}_2^m\delta\tilde{l}_{2s} = -\tau_{m2s}, \end{aligned} \tag{24}$$

where τ_{m1s} and τ_{m2s} denote the control torque of the slow subsystem, and $\delta\tilde{l}_{is}$ is the quasi-steady-state solution of the deflection variable. The above three equations constitute the slow manifold for the singularly perturbed system in (21). If $\delta\tilde{l}_{is}$ is eliminated in (22) by combining (23) and (24), we obtain

$$\begin{aligned}&\Big(ml_{cg}^2 + I + J_{m1} l_o^2 d_1^2 \sin^2\theta/r^2 l_1^2(\theta)\\ &\quad + J_{m2} l_o^2 d_2^2 \sin^2\theta/r^2 l_2^2(\theta)\Big)\ddot{\theta} + \Big(J_{m1} l_o^2 d_1^2 \sin\theta\cos\theta/r^2 l_1^2(\theta)\\ &\quad - J_{m1}(l_o d_1 \sin\theta)^3/r^2 l_1^4(\theta) + J_{m2}(l_o d_2 \sin\theta)^3/r^2 l_2^4(\theta)\\ &\quad + J_{m2} l_o^2 d_2^2 \sin\theta\cos\theta/r^2 l_2^2(\theta)\Big)\dot{\theta}^2 + mgl_{cg}\cos\theta\\ &= \begin{bmatrix} l_o d_1 \sin\theta/rl_1(\theta) & -l_o d_2 \sin\theta/rl_2(\theta)\end{bmatrix}\begin{bmatrix}\tau_{m1s}\\ \tau_{m2s}\end{bmatrix}\\ &= 1/r\,\boldsymbol{J}^T\boldsymbol{\tau}_s, \end{aligned} \tag{25}$$

where $\boldsymbol{\tau}_s := [\tau_{m1s}\ \tau_{m2s}]^T$ is the vector of the control torque of the slow subsystem. This equation may be written in short form as

$$M(\theta)\ddot{\theta} + C(\theta, \dot{\theta}) + G(\theta) = 1/r\,\boldsymbol{J}^T\boldsymbol{\tau}_s.$$

The solution θ for (25) can be denoted as θ_s as it represents the solution for the slow subsystem.

Next, to obtain the dynamic equation for the fast subsystem, let us define the following set of perturbed variables as

$$\xi_i := \delta\tilde{l}_i - \delta\tilde{l}_{is}, \quad z_i := \xi_i, \quad w_i := \epsilon\dot{z}_i, \tag{26}$$

where ξ_i indicates the transient deviation of $\delta\tilde{l}_i$ from $\delta\tilde{l}_{is}$ and $\epsilon \triangleq \sqrt{\mu}$ is a small constant used for time scale expansion via $h = t/\epsilon$, resulting in $w_i = dz_i/dh$. We can obtain the fast part of the dynamics by first subtracting the slow form from the overall dynamics and then by imposing condition $\mu = 0$ (or $\epsilon = 0$) on the resulting equation. The eventual equation for the fast part of the dynamics becomes

$$\begin{aligned}\tau_{m1f} &= -\frac{J_{m1}}{r}\frac{d^2 z_1}{dh^2} - r\tilde{K}_1^m z_1,\\ \tau_{m2f} &= -\frac{J_{m2}}{r}\frac{d^2 z_2}{dh^2} - r\tilde{K}_2^m z_2, \end{aligned} \tag{27}$$

where $\tau_{mif} = \tau_{mi} - \tau_{mis}, \quad i = 1, 2$. This is a boundary layer equation that is implicitly parametrized by the slow variable θ_s.

III. CONTROLLER DESIGN FOR TDJ SYSTEM

A. DESIGN OF COMPOSITE CONTROLLER

Once the dynamic equations of the TDJ system are established, the next step is to design a controller that is consistent with the fast and the slow subsystems. It is well known that the composite controller can be written in the following form:

$$\boldsymbol{\tau} = \boldsymbol{\tau}_s + \boldsymbol{\tau}_f := \begin{bmatrix}\tau_{m1,s}\\ \tau_{m2,s}\end{bmatrix} + \begin{bmatrix}\tau_{m1,f}\\ \tau_{m2,f}\end{bmatrix}, \tag{28}$$

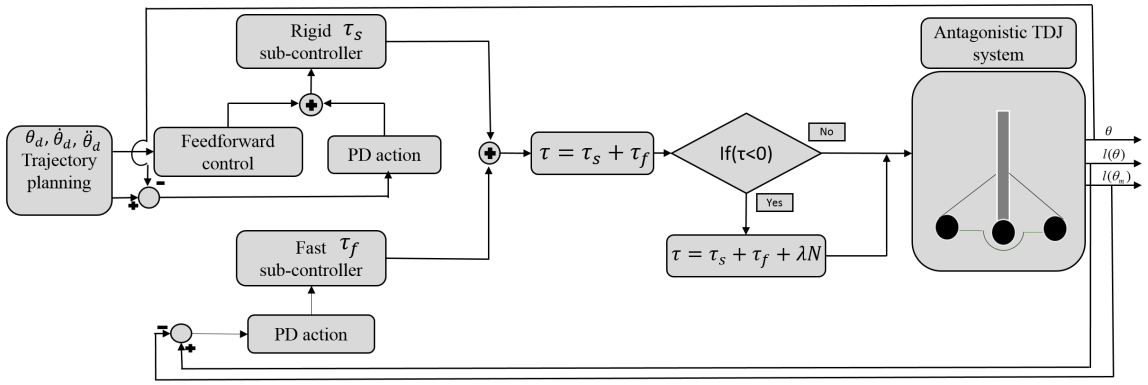

FIGURE 2. Schematic of proposed composite controller for antagonistic TDJ system.

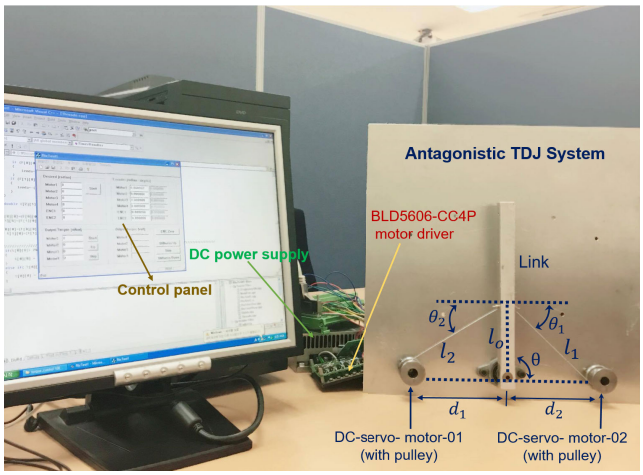

FIGURE 3. Experimental system overview.

TABLE 1. Parameters for the antagonistic TDJ system.

Parameter	Value	Parameter	Value
Tendon length l_1	167 [mm]	Pulley radius	15 [mm]
Tendon length l_2	167 [mm]	Link Inertia	4.99 [gm^2]
Link length l_0	96.02 [mm]	Link mass	537 [g]
Distance $d_1 = d_2$	167 [mm]	Motor Inertia	34.9 [gcm^2]
Motor (R) current	3.04[A]	$K_i{}^m$ $(i = 1, 2)$	9.82E5[N/m]

TABLE 2. Parameters for the controllers in comparison.

Proposed controller	Value	Rigid-only controller	Value
K_{ds}	70 [Nm·s/rad]	K_{ds}	70 [Nm·s/rad]
K_{ps}	13000 [Nm/rad]	K_{ps}	13000 [Nm/rad]
K_{pfi} $(i = 1, 2)$	30000 [N]		
K_{dfi} $(i = 1, 2)$	950 [N·s]		

where $\boldsymbol{\tau}_s$ and $\boldsymbol{\tau}_f$ denote sub-controllers that act upon the slow and fast subsystems, respectively. Each of these sub-controllers can be independently designed to satisfy the stability requirements of the corresponding subsystem. The block diagram of the proposed composite controller is shown in Fig. 2.

For the sub-controller $\boldsymbol{\tau}_s$ for the slow subsystem in (25), the conventional PD control law is employed as

$$\boldsymbol{\tau}_s = r(\boldsymbol{J}^T)^\dagger \left(M(\theta)\ddot{\theta}_d + C(\theta, \dot{\theta}) + G(\theta) + K_{ps}e_\theta + K_{ds}\dot{e}_\theta\right) + \lambda \boldsymbol{N}, \tag{29}$$

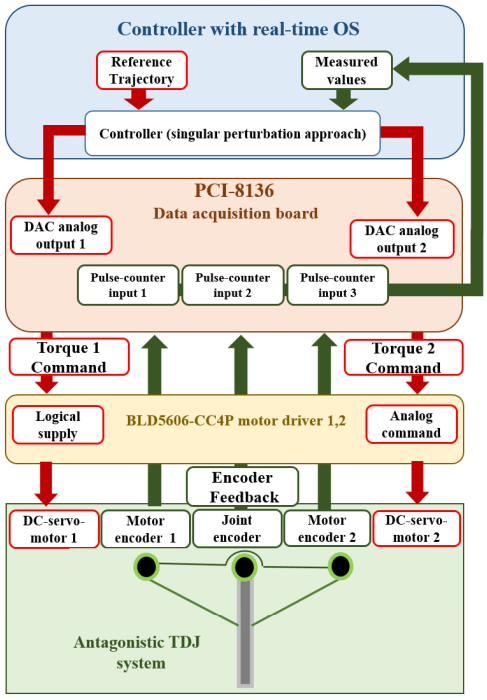

FIGURE 4. Control flow for the experimental system.

where $e_\theta = \theta_d - \theta$ is the trajectory tracking error, K_{ps} and K_{ds} denote positive gains of the PD controller, $(\boldsymbol{J}^T)^\dagger := \boldsymbol{J}(\boldsymbol{J}^T\boldsymbol{J})^{-1}$ represents the pseudo-inverse of $\boldsymbol{J}^T$, and λ and $\boldsymbol{N}$ respectively denote an arbitrary scaling parameter and the one-dimensional null space basis vector of $\boldsymbol{J}^T$ such that $\boldsymbol{J}^T\boldsymbol{N} = 0$. On the right hand side of (29), the first group of terms is the feedforward and feedback compensations, and the last term is the homogeneous input that is chosen in such a way that all components of the input torque are positive, thus preventing slack tendons.

Next, we design the fast sub-controller $\boldsymbol{\tau}_f$ for the fast subsystem in (27). The fast subsystem in a TDJ, if not properly controlled, can jeopardize the entire system, especially for applications that require high precision and high bandwidth operation.

As was the slow sub-controller, the fast sub-controller can take the PD control form:

$$\boldsymbol{\tau}_f = \boldsymbol{K}_{pf}\begin{bmatrix} z_1 \\ z_2 \end{bmatrix} + \boldsymbol{K}_{df}\begin{bmatrix} w_1 \\ w_2 \end{bmatrix}, \tag{30}$$

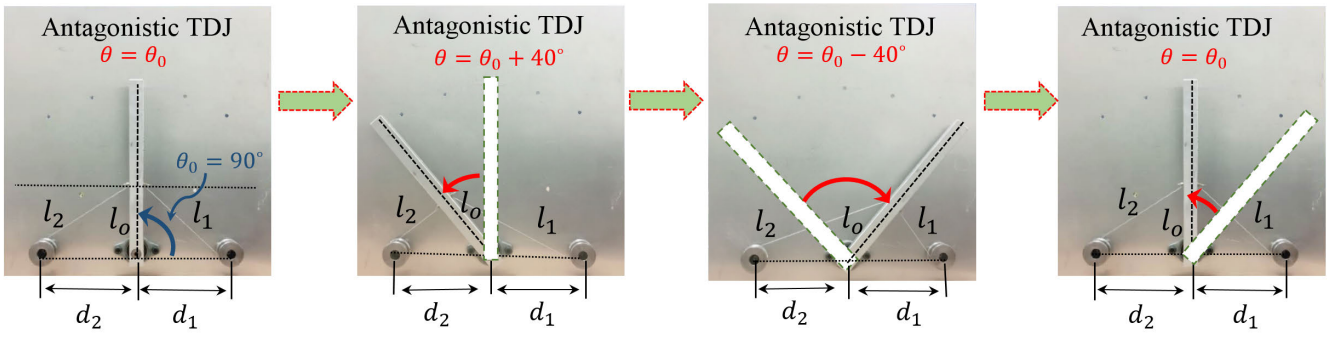

FIGURE 5. Movements of the antagonistic TDJ system while tracking the reference trajectory.

where $\boldsymbol{K}_{pf} \in \mathbb{R}^{2\times 2}$ and $\boldsymbol{K}_{df} \in \mathbb{R}^{2\times 2}$ are the proportional and derivative gain matrices, respectively, of the fast sub-controller.

Note that the control gains $\boldsymbol{K}_{pf}$ and $\boldsymbol{K}_{df}$ should be interpreted as higher gains at normal magnitude and time scales. That is, with feedback δl_i and $\delta \dot{l}_i$, instead of $\delta \tilde{l}_i$ (for z_i) and $d\delta\tilde{l}_i/dh$ (for w_i), the effective gains will become $\boldsymbol{K}_{pf} \to \boldsymbol{K}_{pf}/\mu$ and $\boldsymbol{K}_{df} \to \boldsymbol{K}_{df}/\epsilon$. The main reason why higher gains are required for the fast sub-controller is that the fast subsystem needs to quickly converge to the slow manifold and remain on the equilibrium trajectory. It should also be recalled that (27) is a set of linear parameter varying equations in the fast time scale, which thus requires the condition on gains, $\boldsymbol{K}_{pf}$ and $\boldsymbol{K}_{df}$, to ensure stability. We shall discuss this issue in the next subsection.

Ultimately, our composite controller can be constructed by adding a corrective term (*i.e.,* the fast sub-controller) to the slow sub-controller as follows:

$$\boldsymbol{\tau} = r(\boldsymbol{J}^T)^\dagger \left(M(\theta)\ddot{\theta}_d + C(\theta,\dot{\theta}) + G(\theta) + K_{ps}e_\theta + K_{ds}\dot{e}_\theta\right) + \boldsymbol{K}_{pf}\begin{bmatrix} z_1 \\ z_2 \end{bmatrix} + \boldsymbol{K}_{df}\begin{bmatrix} w_1 \\ w_2 \end{bmatrix} + \lambda \boldsymbol{N}. \quad (31)$$

It should be remembered that the output tension for the proposed composite controller (31) can be guaranteed to be positive with a suitable choice of λ.

B. STABILITY ANALYSIS

Now that we have the two reduced-order subsystems in (25) and (27), and their respective sub-controllers in (29) and (30),

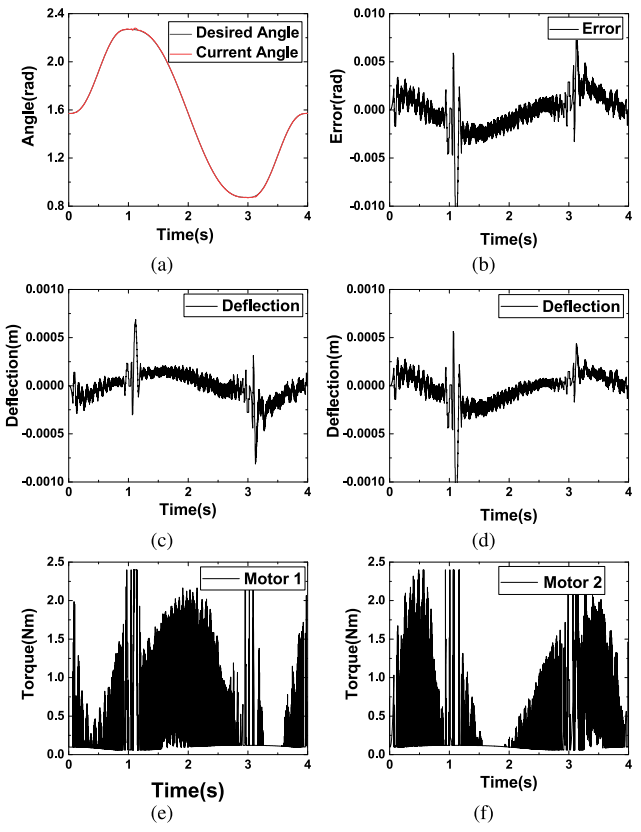

FIGURE 6. Experimental results for the rigid-only joint controller. (a) Trajectory tracking. (b) Trajectory tracking error. (c) Elastic deflection in l_1. (d) Elastic deflection in l_2. (e) Torque 1. (f) Torque 2.

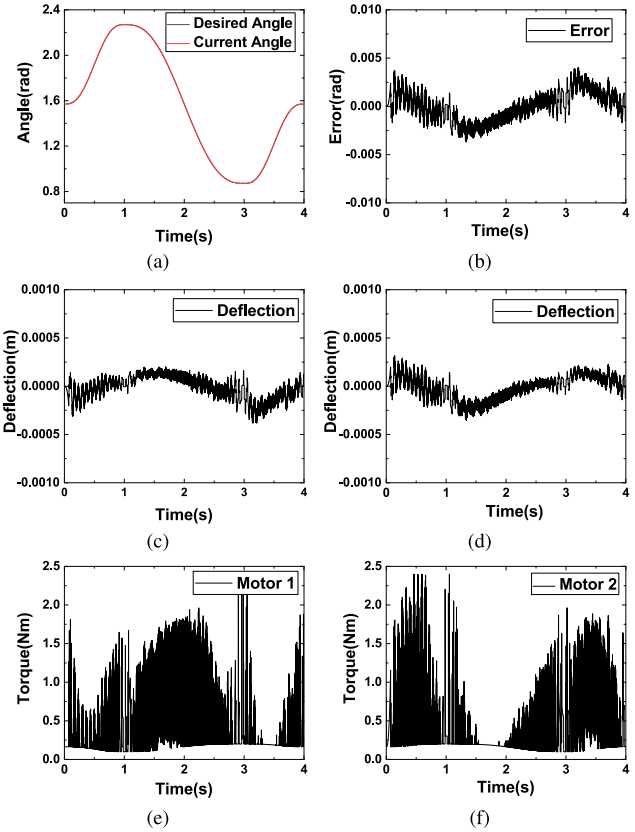

FIGURE 7. Experimental results for the proposed controller. (a) Trajectory tracking. (b) Trajectory tracking error. (c) Elastic deflection in l_1. (d) Elastic deflection in l_2. (e) Torque 1. (f) Torque 2.

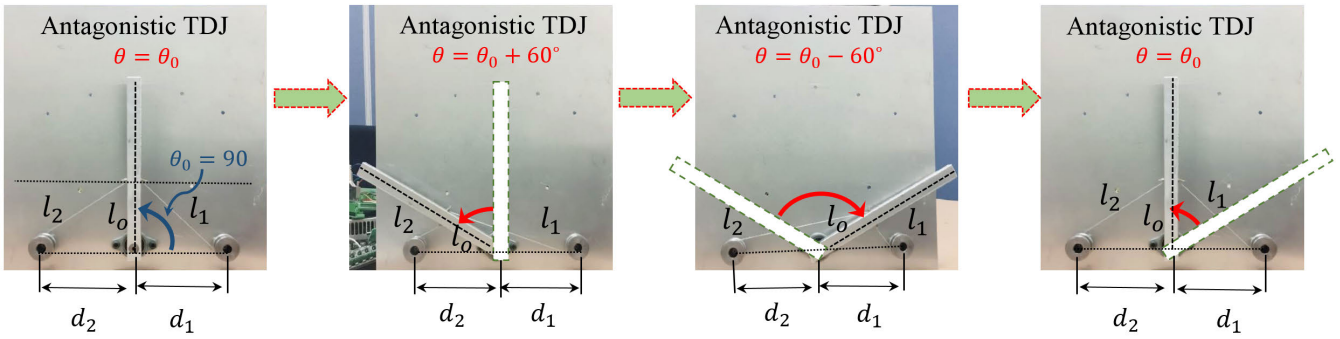

FIGURE 10. Movements of the antagonistic TDJ system while tracking the reference trajectory (extended range of joint motion).

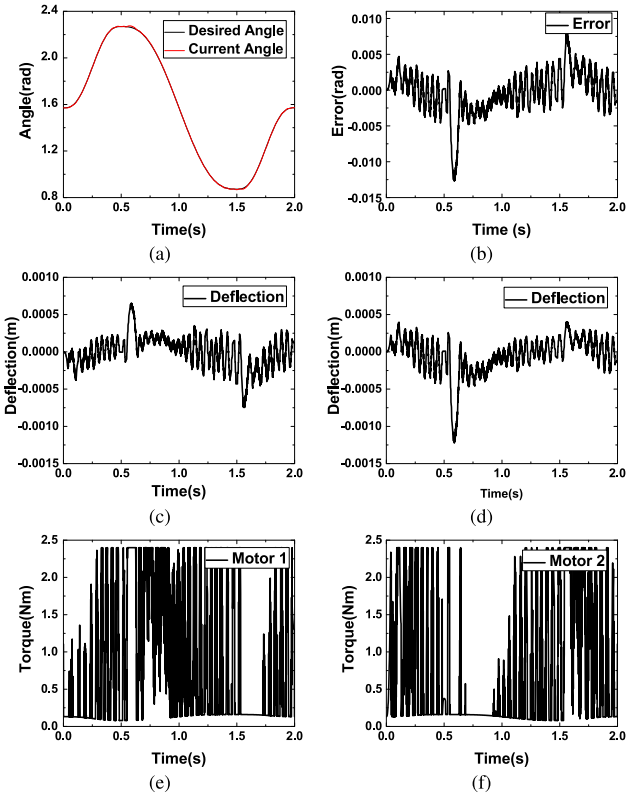

FIGURE 8. Experimental result by using rigid-only joint controller (faster trajectory). (a) Trajectory tracking. (b) Trajectory tracking error. (c) Elastic deflection in l_1. (d) Elastic deflection in l_2. (e) Torque 1. (f) Torque 2.

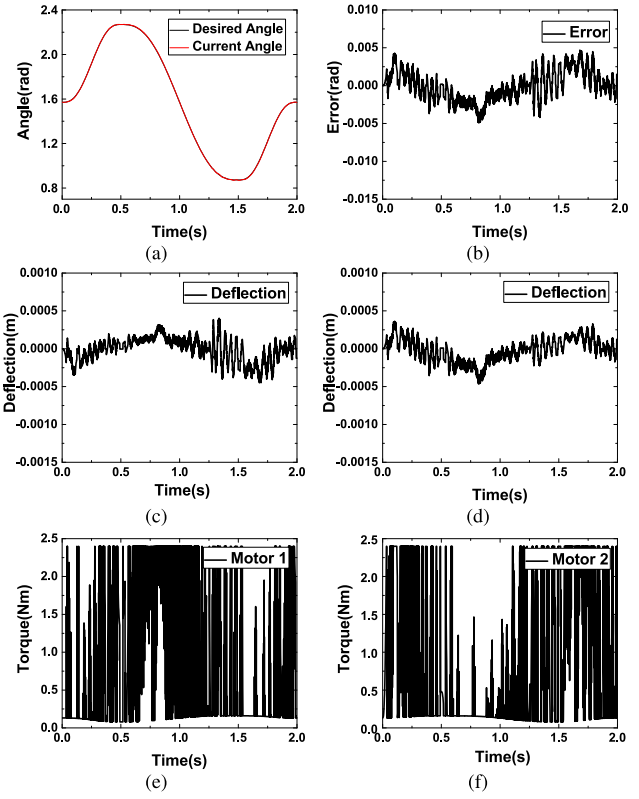

FIGURE 9. Experimental result by using the proposed controller (faster trajectory). (a) Trajectory tracking. (b) Trajectory tracking error. (c) Elastic deflection in l_1. (d) Elastic deflection in l_2. (e) Torque 1. (f) Torque 2.

the stability of the overall system should be discussed. For the slow subsystem, stability using conventional PD control can be guaranteed without any difficulty, as discussed in numerous previous research studies [22], [23]. Therefore, in this section we will focus primarily on the stability of the fast subsystem, and then the combined system. In fact, once the fast subsystem is rendered stable, the stability of the entire system can be guaranteed by invoking Tikhonov's Theorem [27]. According to this theorem, in singularly perturbed systems, if the slow and fast subsystems are independently stable, then the stability of the overall system can be proved using the conditions derived from the stability of the two subsystems [25], [28], [29].

In order to analyze the stability of the fast subsystem, let us recall the fast sub-dynamic equations in (27) and the fast sub-controller in (30). If we combine these, the resulting closed-loop equations become

$$J_{mi}\frac{d^2 z_i}{dh^2} + rK_{dfi}\frac{dz_i}{dh} + (rK_{pfi} + r^2\tilde{K}_i^m)z_i = 0 \quad i = 1, 2.$$

If we define $\boldsymbol{y}_i := \begin{bmatrix} z_i \\ dz_i/dh \end{bmatrix}$, then the above becomes

$$\frac{d\boldsymbol{y}_i}{dh} = \boldsymbol{A}_i\boldsymbol{y}_i, \tag{32}$$

where

$$\boldsymbol{A}_i = \begin{bmatrix} 0 & 1 \\ -(rK_{pfi} + r^2\tilde{K}_i^m)J_{mi}^{-1} & -rK_{dfi}J_{mi}^{-1} \end{bmatrix} \quad i = 1, 2,$$

and K_{pfi} and K_{dfi} are the diagonal elements of $\boldsymbol{K}_{pf}$ and $\boldsymbol{K}_{df}$, respectively. In contrast to previous research in [22]–[24], where $\boldsymbol{A}_i$ was

assumed to be constant, the $\boldsymbol{A}_i$ in our case varies because the stiffness coefficients of the tendons are a function of the joint angle.

The stability of the fast subsystem can be examined using the Lyapunov stability theory. Let a Lyapunov function candidate be

$$V_f = \sum_{i=1}^{2} \boldsymbol{y}_i^T \boldsymbol{P}_i \boldsymbol{y}_i,$$

where

$$\boldsymbol{P}_i = \frac{1}{2}\begin{bmatrix} r(rK_{dfi} + K_{pfi} + r\tilde{K}_i^m) & rJ_{mi} \\ rJ_{mi} & J_{mi} \end{bmatrix}.$$

By invoking Schur's complement [30], the positive definiteness of $\boldsymbol{P}_i$ can be ensured only if the following is satisfied:

$$rK_{dfi} + K_{pfi} + r\tilde{K}_i^m > rJ_{mi}. \quad \text{(Cond. 1)}$$

Taking the derivative with respect to the scaled time, then

$$\begin{aligned} \frac{dV_f}{dh} &= \sum_{i=1}^{2} \frac{d\boldsymbol{y}_i^T}{dh}\boldsymbol{P}_i\boldsymbol{y}_i + \boldsymbol{y}_i^T\boldsymbol{P}_i\frac{d\boldsymbol{y}_i}{dh} + \boldsymbol{y}_i^T\frac{d\boldsymbol{P}_i}{dh}\boldsymbol{y}_i \\ &= \sum_{i=1}^{2} -r^2\boldsymbol{y}_i^T(K_{pfi} + (r\tilde{K}_i^m - \frac{1}{2}d\tilde{K}_i^m/dh))\boldsymbol{y}_i \\ &\quad - r\boldsymbol{y}_i^T(K_{dfi} - J_{mi})\boldsymbol{y}_i. \end{aligned}$$

Simply,

$$\frac{dV_f}{dh} = -\sum_{i=1}^{2} \boldsymbol{y}_i^T S_i \boldsymbol{y}_i,$$

where

$$S_i = \begin{bmatrix} r^2(K_{pfi} + (r\tilde{K}_i^m - \frac{1}{2}d\tilde{K}_i^m/dh)) & 0 \\ 0 & r(K_{dfi} - J_{mi}) \end{bmatrix}.$$

Since K_{pfi}, K_{dfi}, and J_{mi} are positive quantities, dV_{if}/dh becomes negative definite if the following conditions hold:

$$K_{dfi} > J_{mi} \quad \text{(Cond. 2)}$$

$$K_{pfi} + r\tilde{K}_i^m - \frac{1}{2}d\tilde{K}_i^m/dh > 0. \quad \text{(Cond. 3)}$$

Eventually, Cond. 1 through Cond. 3 guarantee that the closed-loop system in (32) is asymptotically stable.

After proving the individual stability of the slow subsystem and the boundary layer (*i.e.*, the fast subsystem), we can prove the stability of the complete system via Tikhonov's theorem. This states that, the asymptotic stability of the original system with the composite controller is guaranteed if a singular parameter is chosen such that $0 < \epsilon < \epsilon^*$, where ϵ^* is some number associated with each particular system. Depending on the complexity of the system, the exact value of ϵ^* may or may not be found easily. (If not found easily, ϵ could be tuned by treating it as a control parameter.) For a detailed proof, see [27] and the references therein. Hence, the asymptotic stability of the overall system can be guaranteed by the combined composite control law (31) comprising the slow sub-controller (29) and the corrective fast sub-controller (30).

IV. EXPERIMENTAL RESULTS

A. EXPERIMENTAL SETUP

The purpose of the experimental tests was to first demonstrate the effectiveness of the proposed control scheme for an antagonistic TDJ system and then to examine the mechanical benefits of the TDJ system when carrying a load. For the experiments, the antagonistic TDJ system shown in Fig.3 was employed. Two brushless DC-servomotors (from Faulhaber GmbH and Co.) with

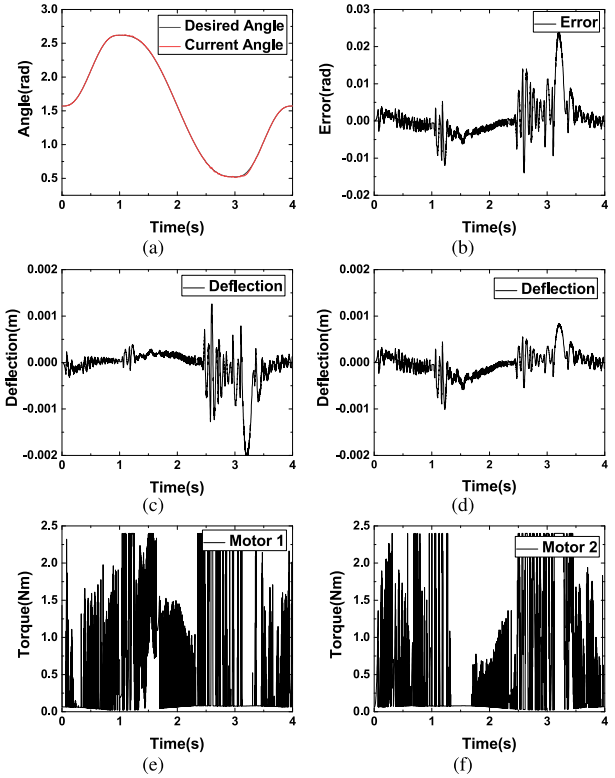

FIGURE 11. Experimental results using the rigid-only joint controller for the extended range of joint motion. (a) Trajectory tracking. (b) Trajectory tracking error. (c) Elastic deflection in l_1. (d) Elastic deflection in l_2. (e) Torque 1. (f) Torque 2.

a 43:1 gear reduction were installed to drive the TDJ system. The motor angles $\theta_{mi}, i = 1, 2$ and the joint angle θ at the bottom of the link were measured using optical rotary incremental encoders (resolution: 1000 counts/rev × 4 decoding). With these encoders, the smallest detectable joint error is approximately 1.57E-3[rad] (*i.e.*, $2\pi/(1000 \times 4)$). The rigid link at the center was pulled by steel tendons (from Carl Stahl Technocables) of diameter 1.0[mm], whose stiffness was computed as $K_i^m = 9.82\text{E}5$[N/m], $i = 1, 2$. Please refer to Table 1 for a summary of the related physical parameters for the TDJ system.

For the implementation of the controller, RTX (Real Time eXtension) from Venturcom Co., patched over Windows XP, was employed as a software platform, running on an IBM PC (Intel Core i5 CPU). The commercial RTX software enabled us to set the timer interrupt with the highest priority, with a maximum latency of only 12μs. The control algorithm in every experimental test was run at 1000Hz. The control flow diagram is depicted in Fig.4.

B. TRACKING CONTROL FOR ANTAGONISTIC TDJ SYSTEM

To verify the effectiveness of the proposed control scheme, we compared the trajectory tracking performance of the rigid-only controller, *i.e.*, the joint PD controller in (29) and that of the proposed composite controller in (31). The rigid-only controller by nature has no ability to cope with the elastic deflection in the tendons. The control parameters used in the experiments are shown in Table 2, with the parameters for the rigid-only controller set to be the same as $\boldsymbol{\tau}_s$ of the proposed controller.

We set the TDJ system to follow a back-and-forth trajectory, as shown in Fig.5. That is, starting at the center with joint angle $\theta_0 = 90°$, the system first moved to the left by 40°, then to the right by 80°, and so on. (Here, for simplicity, the reference trajectories

are described in degrees in the text, but the data plots of the joint angles are displayed in radians.) Fig.6 presents the experimental results using the rigid-only controller. For the back-and-forth joint trajectory, starting at $\theta = 90°$, the overall tracking performance seemed adequate, but joint tracking performance fell rather significantly with noticeable peaks, when the direction of motion changed, as shown in Fig.6(b). The main reason for this behavior has the uncontrolled fast subsystem, in which the elasticity of the tendons was ignored. Any increase in controller gain to reduce the tracking error tended to excite vibrations in the tendons. We observed peaks for tendon deflection exactly when peaks for joint error appeared. (See Figs.6(c)-(d).) The chattering in the control input torques of the motors (see Figs. 6(e)-(f)) was due to the switching between motor 1 and motor 2, as the control action and its subsequent noisy derivative feedback had to maintain positive tension. The chattering in the control input torques may have been mitigated if we had employed encoders with high resolution or velocity observers that could produce smoother velocity profiles.

With the proposed composite controller, the overall control performance improved, as shown in Fig.7. It can be seen that the proposed controller was able to reduce the peaks in joint error that were observed in the previous test with the rigid-only controller. The joint tracking error was bounded by the order of 1E-3[rad], so our proposed controller can guarantee a tracking performance that is almost as accurate as the resolution of the joint encoder (1.57E-3[rad]). The elastic deflection in the tendons also varied monotonously without noticeable peaks, as shown in Figs.7(c)-(d). The magnitude of the chattering in the control input torques was much smaller than that for the rigid-only controller (see Figs.7(e)-(f)).

To further compare control quality, we performed the same set of experiments but reduced the tracking time to 2 seconds for quick motion. As summarized in Figs.8 and 9, the experimental results were very similar to those in the previous set of experiments. The rigid-only controller produced some abrupt peaks in tracking error and elastic deflection when the direction of motion changed, while the proposed controller did not. The maximum tracking error and the elastic deflection increased only slightly as a result of speeding up the trajectory.

Next, we carried out another set of experiments by extending the range of joint motion (Fig.10). The back-and-forth joint path was set to $\pm 60°$ from the center with a 4-second tracking time. This means that the tension of one tendon at the extreme joint angle would become high while that of the other tendon would be much lower. Again, we employed the rigid-only controller and the proposed composite controller in order to compare their effectiveness. Fig.11 presents the experimental results for the rigid-only controller. As can be seen in Fig.11(b), the joint tracking error was characterized by far higher peaks when the direction of joint motion changed compared to that observed in the experiment with the smaller joint angle range, *i.e.*, in Fig.6(b). The tendon deflection also became larger, as shown in Figs.11(c)-(d). The required magnitude of the torques was also larger than that in the previous experiment; refer to Figs.6(e)-(f) and Figs.11(e)-(f) for comparison.

When the proposed composite controller was applied, overall control performance was improved (Fig.12). The proposed controller was able to reduce the peaks in the joint error and tendon deflection, compared to the rigid-only controller (Figs.12(b)-(d)). The severity of the chattering in the control input torques eased as well (Figs.12(e)-(f)).

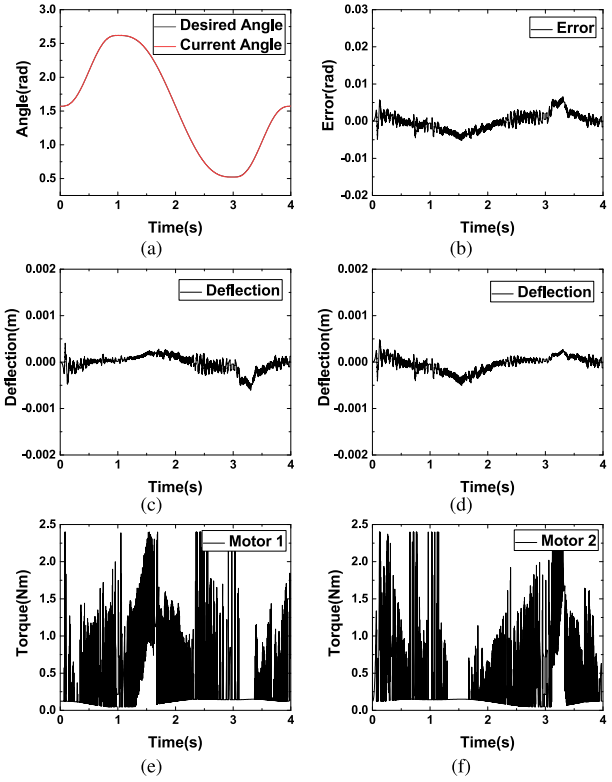

FIGURE 12. Experimental results using the proposed controller for the extended range of joint motion. (a) Trajectory tracking. (b) Trajectory tracking error. (c) Elastic deflection in l_1. (d) Elastic deflection in l_2. (e) Torque 1. (f) Torque 2.

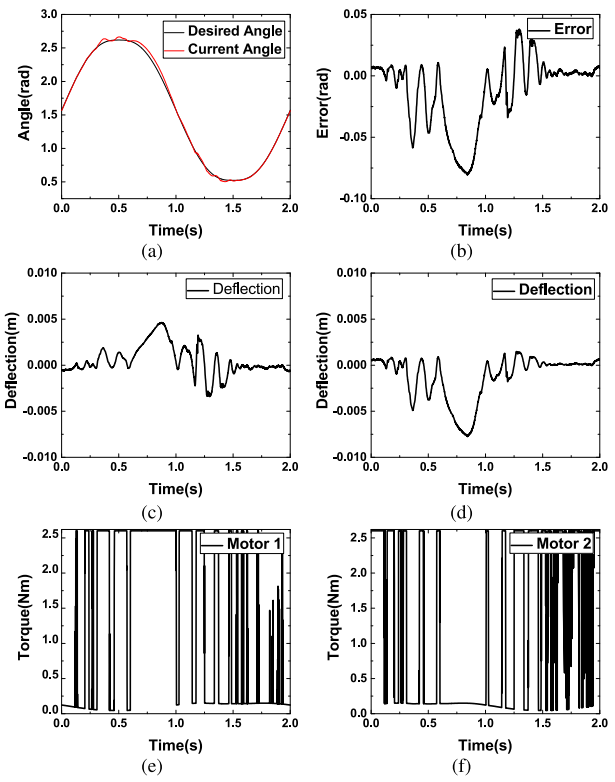

FIGURE 13. Experimental results using the rigid-only joint controller for the extended range of joint motion (faster trajectory). (a) Trajectory tracking. (b) Trajectory tracking error. (c) Elastic deflection in l_1. (d) Elastic deflection in l_2. (e) Torque 1. (f) Torque 2.

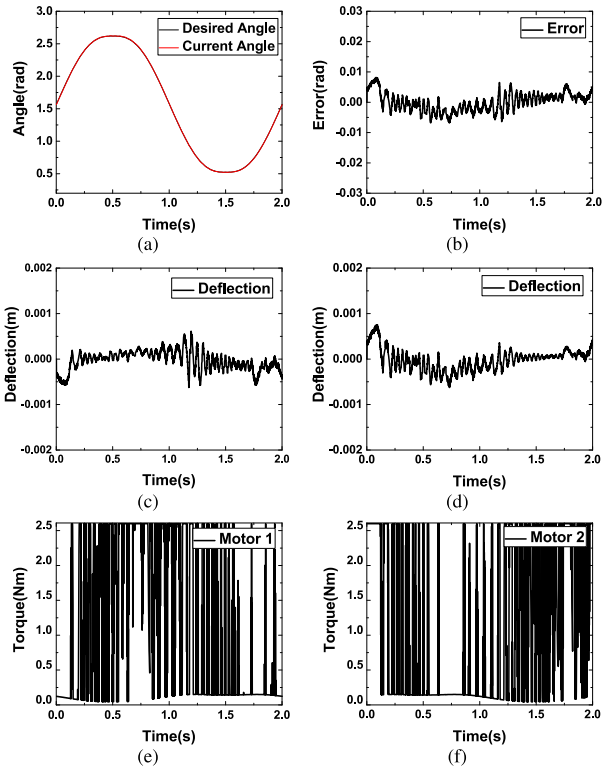

FIGURE 14. Experimental results using the proposed controller for the extended range of joint motion (faster trajectory). (a) Trajectory tracking. (b) Trajectory tracking error. (c) Elastic deflection in l_1. (d) Elastic deflection in l_2. (e) Torque 1. (f) Torque 2.

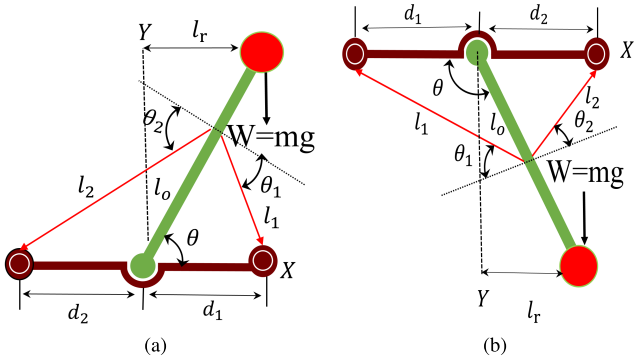

FIGURE 15. Two possible configurations of antagonistic TDJ system. (a) Upright configuration. (b) Suspended configuration.

The above control tasks were tested again for the extended joint path (*i.e.*, a path range of ±60°), but this time for 2 seconds. In this case, the rigid-only controller exhibited noticeable performance degradation, with significant joint error and vibrations in the tendons due to the uncontrolled fast sub-dynamics. As displayed in Fig 13, the maximum tracking error reached nearly 1.0E-2[rad], the tendons were severely wobbling with higher amplitudes, and the control torques did not react adequately to the error, often being clipped off at their physical limits. In contrast, the proposed composite controller still managed to control the total motion in this faster task with an extended range. As presented Fig.14, the tracking error and tendon deflection were kept reasonably low, though their magnitude was slightly larger due to the faster trajectory. The control torques, even when reaching their physical limits, reacted to the error and deflection, unlike with the rigid-only controller.

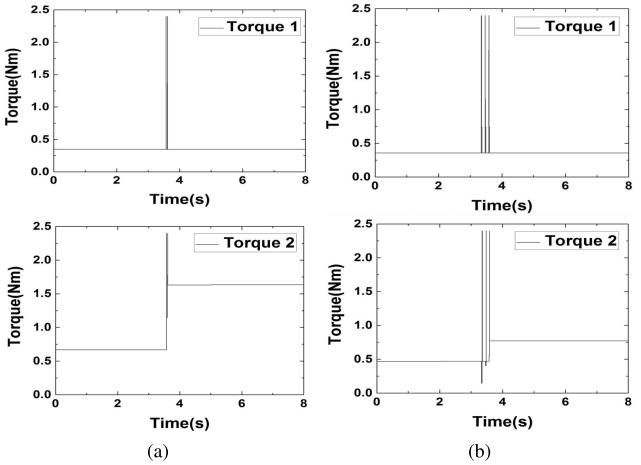

FIGURE 16. Regulatory torques for tension before and after the application of a tip load of 2[kg]. (a) Upright configuration. (b) Suspended configuration.

Overall, these experimental results demonstrate that the composite controller is effective and capable of minimizing joint error and vibration during tracking tasks of an antagonistic TDJ system.

C. LOAD-CARRYING CAPABILITY

The antagonistic TDJ system in Fig.3 allows different load-handling capacities depending on how it is aligned with respect to the gravitational direction. This directional characteristic is unique to TDJs with direct pulls in comparison to prismatic or rotary joints. In this subsection, we verify the differences in load-carrying capacity through experimentation.

First, let us consider two possible arrangements for the antagonistic TDJ system, suspended or upright (Fig. 15). For a tip load of mg, which generates the same moment about the joint axis in both configurations, l_2 works as the main tendon holding the load, while l_1 becomes the conjugate minor tendon. From (1), the required amount of tension in l_2 for both cases, if $t_1 = 0$, is $t_2 = mgl_r/l_0 \cos\theta_2$, where the denominator, $l_0 \cos\theta_2$, which represents the effective moment arm of tension, grows as θ_2 decreases. As indicated in Fig. 15, the suspended configuration requires less tension to hold the tip load than the upright configuration due to a smaller θ_2. The suspended configuration, enjoys this structural advantage for most of the workspace range of the joint, as does the human elbow.

In order to verify the above observation, additional experiments were conducted to compare the load-carrying capacity of the upright and suspended configurations after placing a load of 2[kg] at the tip. In these experiments, the TDJ system was initially set to hold an equilibrium position despite the non-zero action of the internal tendons. A mass of 2[kg] was then placed at the tip about 3.5[s] later. Because the control action was active, the motors driving the tendons managed to adjust their torques to settle on a new equilibrium position and statically balance the added load. The torque profiles before and after the load was added were recorded (Fig.16). The torque for the main tendon (t_2) underwent a step change in its value for both the upright and suspended configurations, while the torque for the conjugate tendon (t_1) was kept constant. The size of the step change in t_2, needed to counteract the external load, differed noticeably for the upright and the suspended configurations. That is, four time more torque was needed for t_2 in the upright configuration than in the suspended one. This experimental result highlights the benefit of suspended configurations in load carrying and handling.

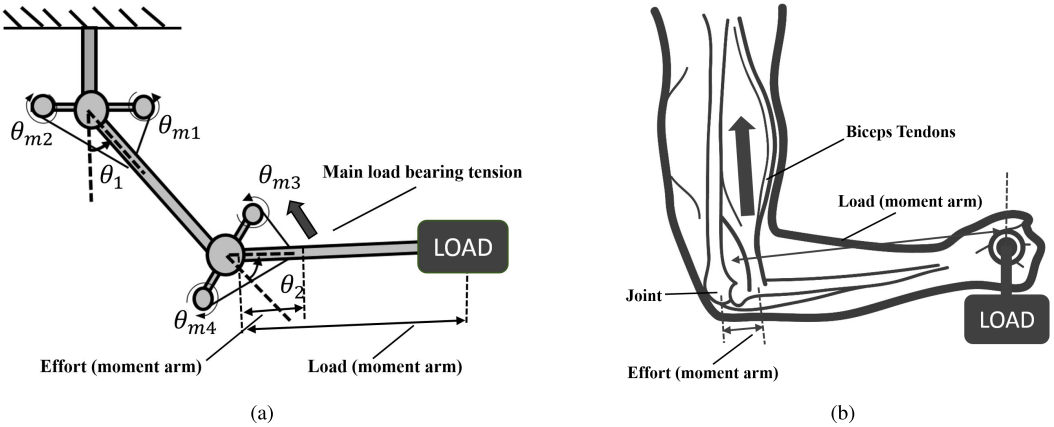

FIGURE 17. Antagonistic TDJ system: Analogy with the human arm. (a) Robotic arm with antagonistic TDJs. (b) Human arm.

This advantage of suspended configurations in antagonistic TDJs can be utilized to build multi-DOF systems like the one shown in Fig.17(a), which is very similar to the human arm (Fig.17(b)). A serial connection of antagonistic TDJs, suspended as shown in Fig.17(a), can produce a large mechanical moment with minimal effort (*i.e.*, tension) in each tendon that is involved in a lifting task, although workspace volume may have to be sacrificed compared to conventional rotary-jointed robotic arms. Because of the resemblance to the human arm and the significant advantage in load-carrying capacity, antagonistic TDJs are appealing design candidates for efficient robotic arms destined to handle heavy loads.

V. CONCLUSION

This paper described the dynamic modeling and controller design of an antagonistic tendon-driven joint (TDJ) system that utilizes elastic tendons. The elasticity of tendons has a negative impact on the performance of TDJ systems due to vibration and poor controllability. In order to cope with this issue, the singular perturbation approach was applied to develop a practical control scheme. Firstly, the equations for the complete dynamics of an antagonistic TDJ system were derived and then the equations for the slow and fast subsystems were extracted from the overall system. A composite controller was then designed that consisted of slow and fast sub-controllers. The stability of the closed loop system was analyzed by applying Tikhonov's theorem. We took into account the internal force to ensure there was no slack in the tendons. The effectiveness of the proposed control scheme was verified through experiments. The experimental results demonstrated that the proposed controller was effective in trajectory tracking tasks under various conditions. The superior load-carrying capacity of the antagonistic TDJ system was also confirmed through experiments.

REFERENCES

[1] K. Müller, C. Reichert, and T. Bruckmann, *Cable-Driven Parallel Robots*. Berlin, Germany: Springer, 2015.

[2] A. Riechel, P. Bosscher, H. Lipkin, and I. Ebert-Uphoff, "Concept paper: Cable-driven robots for use in hazardous environments," in *Proc. Int. Topical Meet. Robot. Remote Syst. Hazardous Environ.*, Mar. 2004, p. 310–316.

[3] E. Nazma and S. Mohd, "Tendon driven robotic hands: A review," *Int. J. Mech. Eng. Robot. Res.*, vol. 1, no. 3, pp. 1520–1532, 2012.

[4] G. Meunier, B. Boulet, and M. Nahon, "Control of an overactuated cable-driven parallel mechanism for a radio telescope application," *IEEE Trans. Control Syst. Technol.*, vol. 17, no. 5, pp. 1043–1054, Sep. 2009.

[5] M. A. Khosravi and H. D. Taghirad, "Dynamic analysis and control of cable driven robots with elastic cables," *Trans. Can. Soc. Mech. Eng.*, vol. 35, no. 4, pp. 543–557, 2011.

[6] K. Salisbury, W. Townsend, B. Ebrman, and D. DiPietro, "Preliminary design of a whole-arm manipulation system (WAMS)," in *Proc. IEEE Int. Conf. Robot. Autom.*, Apr. 1988, pp. 254–260.

[7] L. Zhang, L. Li, Y. Zou, K. Wang, X. Jiang, and H. Ju, "Force control strategy and bench Press experimental research of a cable driven astronaut rehabilitative training robot," *IEEE Access*, vol. 5, pp. 9981–9989, 2017.

[8] V. Potkonjak, K. Jovanovic, B. Svetozarevic, O. Holland, and D. Mikicic, "Modeling and control of a compliantly engineered anthropomimetic robot in contact tasks," in *Proc. Mech. Robot. Conf.*, Aug. 2011, pp. 28–31.

[9] H. Kino, S. Kikuchi, T. Yahiro, and K. Tahara, "Basic study of biarticular muscle's effect on muscular internal force control based on physiological hypotheses," in *Proc. IEEE Int. Conf. Robot. Autom.*, May 2009, pp. 4195–4200.

[10] S.-R. Oh and S. K. Agrawal, "Cable suspended planar robots with redundant cables: Controllers with positive tensions," *IEEE Trans. Robot.*, vol. 21, no. 3, pp. 457–465, Jun. 2005.

[11] B. Zi and S. Qian, *Design, Analysis and Control of Cable-Suspended Parallel Robots and its Applications*. Singapore: Springer, 2017.

[12] A. B. Alp and S. Agrawal, "Cable suspended robots: Feedback controllers with positive inputs," in *Proc. Amer. Control Conf.*, May 2002, pp. 815–820.

[13] R. L. Williams, P. Gallina, and J. Vadia, "Planar translational cable-direct-driven robots," *J. Field Robot.*, vol. 20, no. 3, pp. 107–120, 2003.

[14] S. Qian, B. Zi, and H. Ding, "Dynamics and trajectory tracking control of cooperative multiple mobile cranes," *Nonlinear Dyn.*, vol. 83, nos. 1–2, pp. 89–108, 2015.

[15] M. A. Khosravi and H. D. Taghirad, "Robust PID control of fully-constrained cable driven parallel robots," *Mechatronics*, vol. 24, no. 2, pp. 87–97, 2014.

[16] H. Kino, T. Yahiro, F. Takemura, and T. Morizono, "Robust PD control using adaptive compensation for completely restrained parallel-wire driven robots: Translational systems using the minimum number of wires under zero-gravity condition," *IEEE Trans. Robot.*, vol. 23, no. 4, pp. 803–812, Aug. 2007.

[17] S.-R. Oh, K. Mankala, S. K. Agrawal, and J. S. Albus, "A dual-stage planar cable robot: Dynamic modeling and design of a robust controller with positive inputs," *J. Mech. Des.*, vol. 127, no. 4, pp. 612–620, 2005.

[18] M. H. Korayem, A. Zehfroosh, H. Tourajizadeh, and S. Manteghi, "Optimal motion planning of non-linear dynamic systems in the presence of obstacles and moving boundaries using SDRE: Application on cable-suspended robot," *Nonlinear Dyn.*, vol. 76, no. 2, pp. 1423–1441, 2014.

[19] M. A. Khosravi and H. D. Taghirad, "Robust PID control of cable-driven robots with elastic cables," in *Proc. 1st RSI/ISM Int. Conf. Robot. Mechatronics (ICRoM)*, Feb. 2013, pp. 331–336.

[20] F. Verhulst, *Methods and Applications of Singular Perturbations: Boundary Layers and Multiple Timescale Dynamics*. New York, NY, USA: Springer, 2005.

[21] P. Kokotovic, H. K. Khalil, and J. O'Reilly, *Singular Perturbation Methods in Control: Analysis and Design*. Philadelphia, PA, USA: SIAM, 1987.
[22] M. A. Khosravi and H. D. Taghirad, "Dynamic modeling and control of parallel robots with elastic cables: Singular perturbation approach," *IEEE Trans. Robot.*, vol. 30, no. 3, pp. 694–704, Jun. 2014.
[23] R. Babaghasabha, M. A. Khosravi, and H. D. Taghirad, "Adaptive robust control of fully constrained cable robots: Singular perturbation approach," *Nonlinear Dyn.*, vol. 85, no. 1, pp. 607–620, 2016.
[24] A. Vafaei, M. A. Khosravi, and H. D. Taghirad, "Modeling and control of cable driven parallel manipulators with elastic cables: Singular perturbation theory," in *Proc. Int. Conf. Intell. Robot. Appl.*, Dec. 2011, pp. 455–464.
[25] B. Siciliano and W. J. Book, "A singular perturbation approach to control of lightweight flexible manipulators," *Int. J. Robot. Res.*, vol. 7, no. 4, pp. 79–90, 1988.
[26] J. Cheong, W. K. Chung, and Y. Youm, "Inverse kinematics of multilink flexible robots for high-speed applications," *IEEE Trans. Robot. Autom.*, vol. 20, no. 2, pp. 269–282, Apr. 2004.
[27] H. K. Khalil, *Nonlinear Systems*. Englewood Cliffs, NJ, USA: Prentice-Hall, 2001.
[28] M. Salehi and G. Vossoughi, "Impedance control of flexible base mobile manipulator using singular perturbation method and sliding mode control law," *Int. J. Control, Autom., Syst.*, vol. 6, no. 3, pp. 677–688, 2008.
[29] A. Cavallo and C. Natale, "High-order sliding control of mechanical systems: Theory and experiments," *Control Eng. Pract.*, vol. 12, no. 9, pp. 1139–1149, 2004.
[30] F. Zhang, *The Schur Complement and Its Applications*. New York, NY, USA: Springer, 2005.

MUHAMMAD SHOAIB received the B.S. degree in electronics engineering from the COMSATS Institute of Information Technology Abbottabad, Abbottabad, Pakistan, in 2013, and the M.S. degree from the Department of Control and Instrumentation Engineering, Korea University, Sejong, South Korea, in 2017. His research interests include human-robot cooperation, design, motion control, flexible, and mobile robotic manipulation.

JOONO CHEONG received the B.S., M.S., and Ph.D. degrees from the Pohang University of Science and Technology in 1995, 1997, and 2003, respectively. In 2003, he was a Researcher with the Institute of Precision Machine and Design, Seoul National University, Seoul. From 2003 to 2005, he was a Post-Doctoral Researcher with the Research Laboratory of Electronics, Massachusetts Institute of Technology, Cambridge, MA, USA. Since 2005, he has been with the Department of Control and Instrumentation Engineering, Korea University, Sejong, where he is currently a Professor and also the Director of the Laboratory for Advanced Robotics. His research interests are robotic manipulation, grasping, and mechanical systems control.

DONG IL PARK received the B.S. and M.S. degrees in mechanical engineering and the Ph.D. degree from the Korea Advanced Institute of Science and Technology in 2000, 2002, and 2006, respectively. Since 2006, he has been with the Korea Institute of Machinery and Materials, where he has been involved in robotics. His research fields are the design, control, and application of robot manipulators and mobile robots.

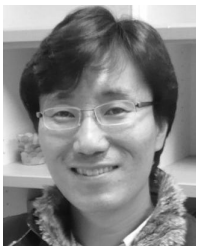

CHAN HUN PARK received the B.S. degree in mechanical engineering from Yeungnam University, South Korea, in 1994, the M.S. degree in mechanical engineering from the Pohang University of Science and Technology, South Korea, in 1996, and the Ph.D. degree from the Korea Advanced Institute of Science and Technology, in 2010. Since 1996, he has been with the Korea Institute of Machinery and Materials, South Korea, where he is currently a Senior Researcher. His research fields include human–robot cooperation and design and control of dual arm robot manipulator for industrial applications.